JOURNAL OF GEOPHYSICAL RESEARCH, VOL. 92, NO. C7, PAGES 6966–6970, JUNE 30, 1987

An Instability Theory of Ice-Air Interaction for the Formation of Ice Edge Bands

P. C. CHU

Department of Oceanography, Naval Postgraduate School, Monterey, California

Ice edge bands are well-observed phenomena at the ice edge of the world ocean at times when winds are blowing off the ice. Differing from the wave radiation theory, water wave theory, wind wave theory, and ice-water coupling theory, we propose an ice-air feedback mechanism to generate the ice edge bands. To eliminate ocean effects, the water is set motionless. Thermally generated surface winds, blowing from ice to water (ice breeze) with some deflection due to the earth's rotation, force the drift of ice floes in the marginal ice zone (MIZ). By changing the surface temperature gradient, the ice motion feeds back on the surface winds. A coupled ice-air model similar to the author's earlier paper is employed to discuss the instability properties of such a feedback mechanism. The linearized governing equations are then solved as an eigenvalue problem with two model parameters: mean ice thickness H_i (0.5 m $< H_i <$ 2.5 m) and a characteristic surface temperature difference over ice and water DT_0 (4°C $< DT_0 <$ 20°C). The model results show alternating ice divergence and convergence zones and demonstrate a great number of e-folding acceleration modes excited by the coupled ice-air system. Ice floes are transported from the divergence area to the convergence zone and are eventually rearranged into a band structure. The e-folding acceleration rate of ice motion depends on the width of two adjacent convergence zones l. It increases with L/l (where L is the length of twice the MIZ width, i.e., 200 km) for 10 km $< l <$ 200 km, and then remains high for 2 km $< l <$ 10 km. The length scale (2–10 km) of the high acceleration modes agrees well with the observed ice edge bandwidth (1–10 km). The e-folding acceleration rate increases with an increase in DT_0 and with a decrease in H_i.

1. INTRODUCTION

Surface bands of ice floes are generally observed at ice edges of the world ocean when winds are blowing off the ice. These bands have size scales of 1–10 km, with their long axes oriented approximately normal to the wind direction. The ice band spacing varies strongly from 1 to 10 km. Differing from wave radiation theory [*Wadhams*, 1983], water wave theory [*Muench et al.*, 1983], wind wave theory [*Martin et al.*, 1983], and ice-water coupling theory [*Häkkinen*, 1986], we propose in this study an ice-air feedback mechanism for the generation of ice edge bands in the marginal ice zone (MIZ) by means of an ice-air model similar to that treated by *Chu* [1986*a*] except that (1) no horizontal eddy viscosity ν_h is included in the boundary layer airflow model and (2) the solutions are not restricted to the first Fourier mode.

McPhee [1980] mentioned ice-ocean and ice-air coupling in a review paper. A possible mechanism for the mesoscale ice-air interaction is presented in Figure 1. Surface winds generated by the surface temperature gradient blow from ice to water (ice breeze) with some deflection due to the earth's rotation. However, movement of ice floes in the MIZ changes thermal conditions near the surface and produces a different surface temperature gradient across the ice edge, which in general is less than or greater than the characteristic temperature gradient in the MIZ.

The ice-air interaction model depicted in the subsequent sections is intended to determine the unstable modes of ice motion and to predict the length scale of the ice band spacing.

2. THERMALLY FORCED BOUNDARY LAYER AIR FLOW

Overland et al. [1983] show that air temperature increases waterward in the Bering Sea MIZ (Figure 2). Such a surface temperature gradient will thermally generate local atmospheric flow near the MIZ. In this section we utilize a planetary boundary layer air model treated by *Kuo* [1973] and *Chu* [1986*a*, *b*, *c*] to simulate thermally forced boundary layer airflow. The x axis is in the cross-edge direction, and the y axis is parallel to the ice edge, as is shown in Figure 3.

The potential temperature of air is divided into two parts: a basic state $\theta_{B*}(z)$ and perturbation θ_*'. The basic state is given by

$$\theta_{B*}(z) = \theta_{B0} + (N^2\theta_{B0}\delta/g)z \tag{1}$$

where θ_{B0} is the basic air potential temperature at the surface and N is the Brunt-Väisälä frequency. The subscript asterisk means dimensional variables.

As discussed by *Chu* [1986*a*], the waterward/iceward migration of the MIZ increases/decreases the surface temperature gradient, so the effects of ice flow on the surface air temperature gradient can be parameterized as

$$\partial^2\theta_{a*}'/\partial t_*\,\partial x_* = (\pi DT_0/L^2)u_{i*}(x_*, t_*) \tag{2}$$

where DT_0 is the characteristic surface temperature difference across the MIZ and L is a length scale twice the MIZ width; subscripts a and i denote air and ice, respectively.

The coordinates and atmospheric variables are nondimensionalized by setting

$$\begin{gathered}(x_*, z_*, t_*) = (xL, z\delta, tT) \qquad s' = \theta_{a*}'/\theta_{B0} = (DT_0/\theta_{B0})s_a \\ (u_{a*}, v_{a*}, w_{a*}, u_{i*}, v_{i*}) = U(u_a, v_a, w_a\,\delta/L, u_i, v_i) \\ P_{a*} = (g\delta DT_0/\theta_{B0})p_a \qquad \delta = (\nu/\Omega)^{1/2}\end{gathered} \tag{3}$$

where ν is the vertical eddy viscosity, Ω is the angular velocity of the earth's rotation,

$$U \equiv g\delta DT_0/(2L\Omega\theta_{B0}) \tag{4}$$

Paper number 7C0013.
0148-0227/87/007C-0013$05.00

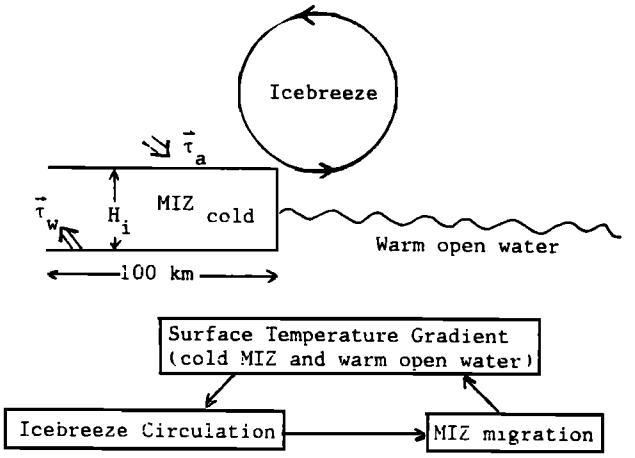

Fig. 1. Ice-air-ocean coupled system.

is the scale of ice breeze wind, and $T = L/U$ is the time scale for change of the surface temperature gradient due to movement of the ice edge. If we assume that local airflow satisfies the modified Boussinesq approximation [*Kuo*, 1973] then the vorticity equation, the momentum equation (both in the y direction), and the heat equation for air disturbances generated by the differential surface temperature gradient near the MIZ are [*Chu*, 1986*a*]

$$E\partial^2(\nabla^2\psi_a)/\partial z^2 = f_0\partial v_a/\partial z - \partial s_a/\partial x \tag{5}$$

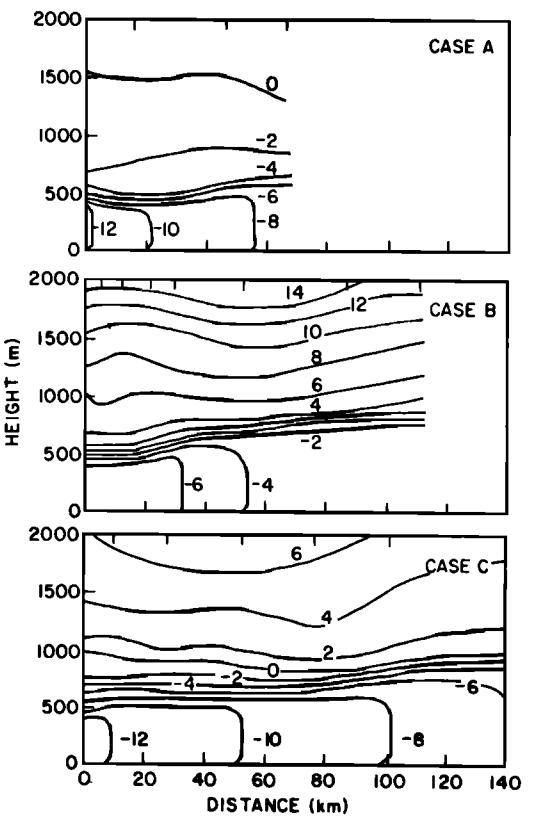

Fig. 2. Cross sections of potential temperature perpendicular to the ice edge in the Bering Sea for the three off-ice wind cases [from *Overland et al.*, 1983].

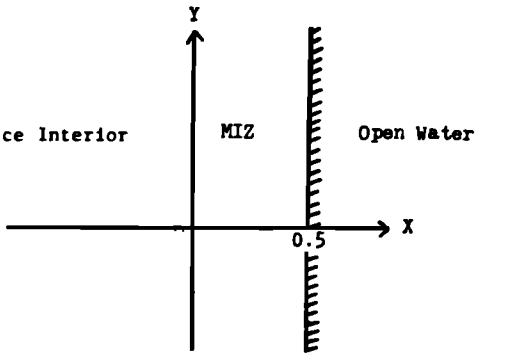

Fig. 3. The model MIZ and the coordinate system.

$$E\partial^2 v_a/\partial z^2 = -f_0\partial\psi_a/\partial z \tag{6}$$

$$E\partial^2 s_a/\partial z^2 = Ri\ \partial\psi_a/\partial x \tag{7}$$

In the foregoing,

$$u_a = -\partial\psi_a/\partial z \qquad w_a = \partial\psi_a/\partial x$$
$$\nabla^2 \equiv \delta^2/L^2\partial^2/\partial x^2 + \partial^2/\partial z^2 \tag{8}$$

where $f_0 = \sin\phi$, ϕ is latitude, and

$$E \equiv \nu/(2\Omega\delta^2) = \tfrac{1}{2} \qquad Ri \equiv \delta^2 N^2/(4L^2\Omega^2) \tag{9}$$

are the Ekman and Richardson numbers, respectively.

The model variables are decomposed into Fourier sine or cosine series:

$$\psi_a(x, z, t) = \sum_{k=1}^{\infty} \psi_{ak}(z, t) \sin k\pi x \tag{10a}$$

$$s_a|_{z=0} = \sum_{k=1}^{\infty} s_{ak}(t) \cos k\pi x \tag{10b}$$

$$u_a|_{z=0} = \sum_{k=1}^{\infty} u_{ak}(t) \sin k\pi x$$
$$v_a|_{z=0} = \sum_{k=1}^{\infty} v_{ak}(t) \sin k\pi x \tag{10c}$$

$$u_i = \sum_{k=1}^{\infty} u_{ik}(t) \sin k\pi x$$
$$v_i = \sum_{k=1}^{\infty} v_{ik}(t) \sin k\pi x \tag{10d}$$

Introducing a new variable ζ_i representing nondimensional ice displacement in the x direction,

$$L\, d\zeta_i/dt = u_i \tag{11}$$

expanding it into Fourier sine series,

$$\zeta_i(x, t) = \sum_{k=1}^{\infty} \zeta_{ik}(t) \sin k\pi x \tag{12}$$

and substituting (10*d*) and (12) into (11), we obtain

$$L\, d\zeta_{ik}/dt = u_{ik} \tag{13}$$

Integrating (2) with respect to x and t after nondimensionalization, we get

$$s_{ak}(t) = -[\zeta_{ik}(t) + \beta_k]/k \tag{14}$$

where β_k ($k = 1, 2, \cdots$) are the integration constants.

Eliminating v_a and s_a from (5)–(7), we find that the stream function satisfies the following partial differential equation:

$$(1/4\partial^4/\partial z^4 + f_0^2)\,\partial^2\psi_a/\partial z^2 + Ri\,\partial^2\psi_a/\partial x^2 = 0 \qquad (15)$$

We solve (15) for the stream function ψ_a and obtain the solutions of v_a and s_a from (6) and (7) after substituting ψ_a. The local airflow is thermally forced by the surface temperature gradient, as is indicated in (14). The boundary conditions in the vertical direction are derived as follows. The dependent variables should remain finite as $z \to \infty$, i.e.,

$$\lim_{z\to\infty} (|\psi_a|, |\partial\psi_a/\partial z|, |v_a|, |s_a|) < \infty \qquad (16)$$

The boundary conditions at $z = 0$ are

$$\psi_a = 0 \qquad \partial\psi_a/\partial z = M\,\partial^2\psi_a/\partial z^2$$
$$v_a = M\,\partial v_a/\partial z \qquad s_a = -\sum_{k=1}^{\infty} [\zeta_{ak}(t) + \beta_k] \cos k\pi x/k \qquad (17)$$

where M is a measure of the effective depth of the constant stress sublayer [*Kuo*, 1973]: $M = \nu/(C_{a*}\delta)$, where C_{a*} is a dimensional (meters per second) air drag coefficient.

Substituting (10*a*) into (15), we obtain the following sixth-order ordinary differential equations for the Fourier coefficients ψ_{ak}:

$$d^6\psi_{ak}/dz^6 + 4f_0^2 d^2\psi_{ak}/dz^2 - 4\pi^2k^2\,Ri\,\psi_{ak} = 0 \qquad (18)$$

The general solutions of (18) have the following form:

$$\psi_{ak}(z, t) = (\zeta_{ik} + \beta_k)\sum_{j=1}^{6} a_{kj} \exp(\lambda_{kj}z) \qquad (19)$$

where the eigenvalues λ_{kj} ($j = 1, 2, \cdots, 6$) are the roots of the sixth-order algebraic equations:

$$\lambda^6 + 4f_0^2\lambda^2 - 4k^2\pi^2\,Ri = 0 \qquad (20)$$

According to the upper boundary conditions listed in (16), we must set up coefficients that correspond to those eigenvalues with the positive real parts to zero. Consequently, the general solutions (19) satisfying the top boundary conditions may be written

$$\bar{\psi}_{ak}(z, t) = [\zeta_{ik}(t) + \beta_k]\sum_{j=1}^{3} a_{kj} \exp(\lambda_{kj}z) \qquad (21)$$

where the eigenvalues λ_{kj} all have negative real parts. Substituting (21) into (10*a*), we obtain the stream function

$$\psi_a(x, z, t) = \sum_{j=1}^{3} a_{kj}[\bar{\zeta}_{ik} + \beta_k] \exp(\lambda_{kj}z) \sin k\pi x \qquad (22)$$

Using the definition of a stream function and integrating the momentum equation (6) and the heat equation (7) with respect to z after substituting (22), we find that

$$u_a|_{z=0} = \sum_{k=1}^{\infty} \bar{u}_{ak}[\zeta_{ik} + \beta_k] \sin k\pi x$$
$$v_a|_{z=0} = \sum_{k=1}^{\infty} \bar{v}_{ak}[\zeta_{ik} + \beta_k] \sin k\pi x \qquad (23)$$

$$s_a|_{z=0} = \sum_{k=1}^{\infty} \bar{s}_{ak}[\zeta_{ik} + \beta_k] \cos k\pi x \qquad (24)$$

where

$$\bar{u}_{ak} \equiv \sum_{j=1}^{3} a_{kj}\lambda_{kj} \qquad \bar{v}_{ak} \equiv b_k - 2f_0\sum_{j=1}^{3} a_{kj}/\lambda_{kj}$$
$$\bar{s}_{ak} \equiv 2k\pi R_i\sum_{j=1}^{3} a_{kj}/\lambda_{kj}^2 \qquad (25)$$

Substituting solutions (22)–(24) into the surface boundary conditions listed in (17), we get the following four algebraic equations for a_{kj} an b_k:

$$\sum_{j=1}^{3} a_{kj} = 0$$
$$\sum_{j=1}^{3} \lambda_{kj}(1 - M\lambda_{kj})a_{kj} = 0$$
$$-2f_0\sum_{j=1}^{3} \frac{1 - M\lambda_{kj}}{\lambda_{kj}} a_{kj} + b_k = 0 \qquad (26)$$
$$2k\pi R_i\sum_{j=1}^{3} a_{kj}/\lambda_{kj}^2 = -1/k$$

3. FREE ICE DRIFT MODEL

The linearized momentum equations for a free drift ice model are

$$\partial u_i/\partial t = -\bar{C}_w u_i + fv_i + \bar{C}_a\sum_{k=1}^{\infty} \bar{u}_{ak}[\zeta_{ik}(t) + \beta_k] \sin k\pi x \qquad (27)$$

$$\partial v_i/\partial t = -\bar{C}_w v_i - fu_i + \bar{C}_a\sum_{k=1}^{\infty} \bar{v}_{ak}[\zeta_{ik}(t) + \beta_k] \sin k\pi x \qquad (28)$$

where the first and last terms on the right-hand side represent the water and air stresses on ice, respectively. Here

$$\bar{C}_a \equiv \rho_a C_{a*}/(\rho_i H_i) \qquad \bar{C}_w \equiv \rho_w C_{w*}/(\rho_i H_i) \qquad (29)$$

C_{w*} is a dimensional (meters per second) water drag coefficient (on ice), and ρ_a, ρ_i, and ρ_w are the densities of air, ice, and water, respectively.

4. UNSTABLE MODES OF ICE MOTION

The solutions of (27)–(28) have the following forms:

$$u_i(x, t) = \sum_{k=1}^{\infty} \bar{u}_{ik} \exp(\sigma_k t) \sin k\pi x \qquad (30)$$

$$v_i(x, t) = \sum_{k=1}^{\infty} \bar{v}_{ik} \exp(\sigma_k t) \sin k\pi x \qquad (31)$$

Substituting (30) and (31) into (27) and (28), we obtain the following dispersion relation:

$$\sigma_k^3 + 2\bar{C}_w\sigma_k^2 + [\bar{C}_w^2 - \bar{C}_a\bar{u}_{ak}/L + f^2]\sigma_k - (\bar{C}_a/L)[\bar{C}_w\bar{u}_{ak} + f\bar{v}_{ak}] = 0 \qquad (32)$$

The roots σ_k ($k = 1, 2, \cdots$) of the cubic equations (32) give the e-folding time dependence of the kth component of ice velocity. The standard values of model parameters are given in Table 1. The instability criterion for the kth mode of ice motion in the MIZ can be written

$$\text{Re}(\sigma_k) < 0 \qquad (33a)$$

TABLE 1. Standard Model Parameters

Parameter	Value
L	200 km
Ω	0.7292×10^{-4} s^{-1}
ρ_a	1.29 kg/m^3
C_{a*}	3×10^{-2} m/s
ν	5 m^2/s
g	9.81 m/s^2
ρ_w	10^3 kg/m^3
C_{w*}	1.76×10^{-3} m/s
ϕ	65°
θ_{B0}	270 K
ρ_i	910 kg/m^3

the kth mode of ice velocity decreases with time,

$$\text{Re}\,(\sigma_k) = 0 \tag{33b}$$

neutral, and

$$\text{Re}\,(\sigma_k) > 0 \tag{33c}$$

the kth mode of ice velocity increases with time. We define the time-increasing mode of ice velocity as an unstable mode.

The oscillation criterion for the kth mode of ice motion is given by

Nonoscillatory

$$\text{Im}\,(\sigma_k) = 0 \tag{34a}$$

Oscillatory

$$\text{Im}\,(\sigma_k) \neq 0 \tag{34b}$$

We compute all the roots of (32) for different values of the parameters H_i and DT_0, which are organized into two groups: (1) fixed H_i (1.5 m), $DT_0 = 4°C$, 8°C, 12°C, 16°C, and 20°C and (2) fixed DT_0 (10°C), $H_i = 0.5$, 1, 1.5, 2, and 2.5 m. We obtain three roots $\sigma_1(k)$, $\sigma_2(k)$, and $\sigma_3(k)$ for each given k, H_i, and DT_0. Here $\sigma_1(k)$ is real and positive for all given k, H_i, and DT_0. However, $\sigma_2(k)$ and $\sigma_3(k)$ are complex with negative real parts. Therefore the time-increasing modes of ice velocity are those eigenfunctions associated with the eigenvalues $\sigma_1(k)$:

$$\begin{aligned} \tilde{u}_{ik}(x, t) &= \bar{u}_{ik} \exp\,[\sigma_1(k)t] \sin k\pi x \\ \tilde{v}_{ik}(x, t) &= \bar{v}_{ik} \exp\,[\sigma_1(k)t] \sin k\pi x \end{aligned} \tag{35}$$

which indicate that the ice velocity $\mathbf{V}_{ik} = (\tilde{u}_{ik}, \tilde{v}_{ik})$ has an e-folding acceleration and a sinusoidal-type spatial variation.

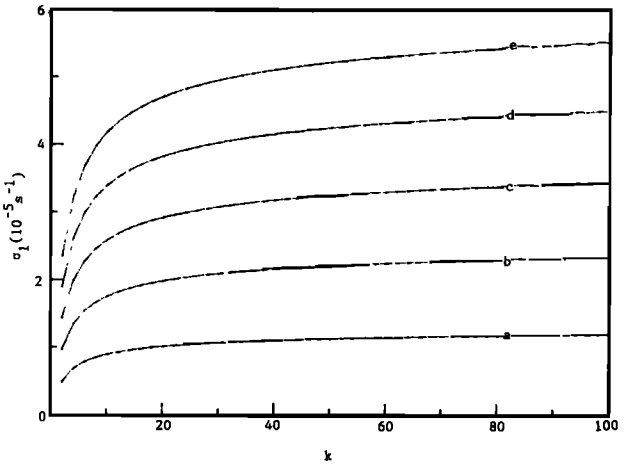

Fig. 5. The $\sigma_1(k)$-k diagram for $H_i = 1.5$ m and (*a*) $DT_0 = 4°C$, (*b*) $DT_0 = 8°C$, (*c*) $DT_0 = 12°C$, (*d*) $DT_0 = 16°C$, and (*e*) $DT_0 = 20°C$.

5. Model Results

Solutions (35) show that time and spatial variations of ice velocity are separable, which means that the sinusoidal-type spatial structure does not change with time and that the e-folding acceleration does not vary with space.

Figure 4 indicates the spatial variation (sinusoidal) of the kth mode ice velocity $\mathbf{V}_{ik}$ depicted in (35). We see the alternation pattern of ice convergence and divergence zones. The width of the two adjacent convergence zones is L/k. Such an ice velocity field transports ice floes from the divergence area to the convergence zones and eventually forms ice edge bands with band spacing L/k.

Solutions (35) also show that this convergence-divergence alternation pattern has an e-folding time variation. The e-folding acceleration factor $\sigma_1(k)$ denotes how fast the ice velocity increases. Figures 5 and 6 are the σ_1-k diagram for groups 1 and 2 of parameters H_i and DT_0, respectively. "Γ-type" curves demonstrate the following facts.

1. For any given parameters H_i and DT_0, the e-folding acceleration factor σ_1 increases rapidly with k when $1 < k < 20$ and then remains high for $20 < k < 100$. This means that the modes with fast increasing ice velocity have short band spacing (2 km $< L/k <$ 10 km).

2. For fixed H_i (1.5 m), the e-folding acceleration rate σ_1 increases with DT_0, since the larger DT_0 is, the stronger the forcing.

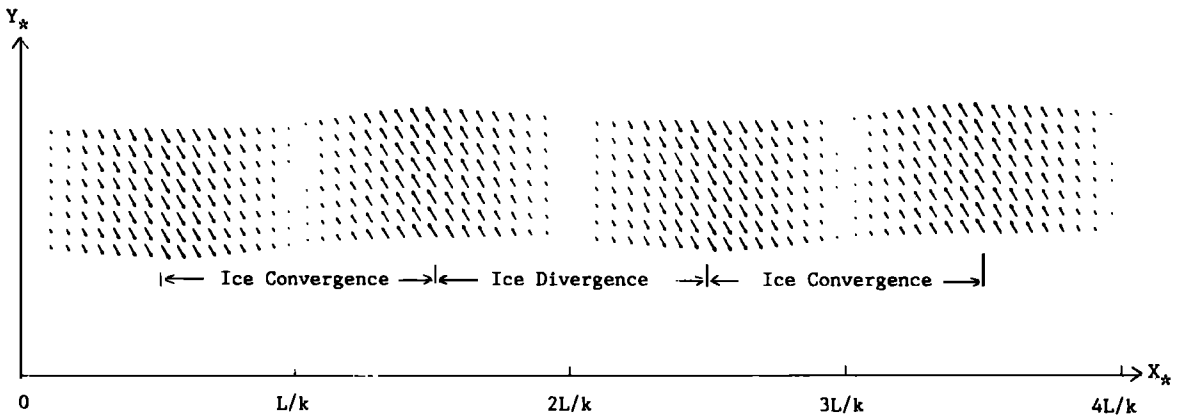

Fig. 4. The kth mode of ice velocity.

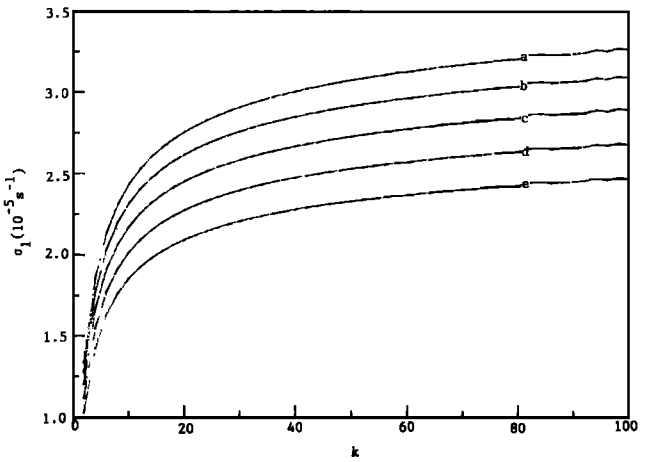

Fig. 6. The $\sigma_1(k)$-k diagram for $DT_0 = 10°C$ and (*a*) $H_i = 0.5$ m, (*b*) $H_i = 1$ m, (*c*) $H_i = 1.5$ m, (*d*) $H_i = 2$ m, and (*e*) $H_i = 2.5$ m.

3. For fixed DT_0 (10°C), the *e*-folding acceleration rate σ_1 increases with a decrease in H_i. The smaller H_i is, the more unstable the coupled system.

4. The *e*-folding acceleration rate for the most unstable modes is around $1–4 \times 10^{-5}$ s^{-1}, and the doubling time during which the ice doubles its speed is

$$T = \ln 2/\sigma_1 \tag{36}$$

Therefore the doubling time for most unstable modes is around 5–20 hours.

6. CONCLUSIONS

1. This ice-air coupled model is intended to depict only the mesoscale processes of ice-air interaction in the MIZ. The synoptic scale pressure gradient may additionally produce surface winds in the MIZ, and large-scale ocean currents may drive ice drift. These processes are, however, beyond the scope of this paper. Nevertheless, where the ice-to-open-water temperature gradient is strong, the mesoscale feedback mechanism discussed here may become as strong as, or stronger than, the synoptic scale and oceanic forcings.

2. The air-ice feedback mechanism in the MIZ generates the alternation pattern of ice convergence and divergence zones. Ice floes are thus transported from the divergence area to the convergence zone and are eventually rearranged into a band structure with spacing as the distance of two adjacent convergence zones.

3. The alternation pattern of ice divergence/convergence has a time variation. The *e*-folding acceleration rate of ice velocity depends on the band spacing. The modes with a fast increasing ice velocity have short band spacing (2 km $< L/k <$ 10 km), which agrees well with the observed ice edge band spacing [*Hakkinen*, 1986; *Martin et al.*, 1983; *Muench et al.*, 1983; *Wadhams*, 1983].

Acknowledgments. The author is grateful to H. L. Kuo and D. R. MacAyeal of the University of Chicago and J. E. Overland and C. H. Pease of the Pacific Marine Environmental Laboratory/NOAA for invaluable discussions and comments. The reviewers' comments are also highly appreciated. This research was supported by grant ATM 83-14206 from the National Science Foundation.

REFERENCES

Chu, P. C., An instability theory of ice-air interaction for the migration of the marginal ice zone, *Geophys. J. R. Astron. Soc.*, *86*, 863–883, 1986*a*.

Chu, P. C., An ice-air feedback mechanism for the migration of the marginal ice zone, *MIZEX Bull. 7*, pp. 54–64, U.S. Army Cold Regions Res. and Eng. Lab., Hanover, N. H., 1986*b*.

Chu, P. C., An air-ice-ocean coupled model for the formation of leads or polynyas, *MIZEX Bull. 7*, pp. 79–88, U.S. Army Cold Regions Res. and Eng. Lab., Hanover, N. H., 1986*c*.

Häkkinen, S., Ice banding as a response of the coupled ice-ocean system to temporally varying winds, *J. Geophys. Res.*, *91*(C4), 5047–5053, 1986.

Kuo, H. L., Planetary boundary layer flow of a stable atmosphere over the globe, *J. Atmos. Sci.*, *30*, 53–65, 1973.

Martin, S., P. Kauffman, and C. Parkinson, The movement and decay of ice edge bands in the winter Bering Sea, *J. Geophys. Res.*, *88*(C5), 2803–2812, 1983.

McPhee, M. G., Physical oceanography of the seasonal sea ice zone, *Cold Region Sci. Technol.*, *2*, 93–118, 1980.

Muench, R. D., P. H. LeBlond, and L. E. Hachmeister, On some possible interactions between internal waves and sea ice in the marginal ice zone, *J. Geophys. Res.*, *88*(C5), 2819–2826, 1983.

Overland, J. E., R. M. Reynolds, and C. H. Pease, A model of the atmospheric boundary layer over the marginal ice zone, *J. Geophys. Res.*, *88*(C5), 2836–2840, 1983.

Wadhams, P., A mechanism for the formation of ice edge bands, *J. Geophys. Res.*, *88*(C5), 2813–2818, 1983.

P. C. Chu, Department of Oceanography, Naval Postgraduate School, Monterey, CA 93943.

(Received June 10, 1986;
accepted December 4, 1986.)